EDGE ARTICLE

Check for updates

Deciphering the chemical bonding of the trivalent oxygen atom in oxygen doped graphene†

Andoni Ugartemendia, [ID] [ab] Irene Casademont-Reig, [ID] [c] Lili Zhao, [ID] [d] Zuxian Zhang, [d] Gernot Frenking, [ID] [bde] Jesus M. Ugalde, [ab] Aran Garcia-Lekue[*df] and Elisa Jimenez-Izal [ID] [*ab]

Recently, planar and neutral tricoordinated oxygen embedded in graphene has been imaged experimentally (*Nat. Commun.*, 2019, **10**, 4570–4577). In this work, this unusual chemical species is studied utilizing a variety of state-of-the-art methods and combining periodic calculations with a fragmental approach. Several factors influencing the stability of trivalent oxygen are identified. A σ-donation and a π-backdonation mechanism between graphite and oxygen is established. π-Local aromaticity, with a delocalized 4c−2e bond involving the oxygen atom and the three nearest carbon atoms aids in the stabilization of this system. In addition, the framework in which the oxygen is embedded is crucial too to the stabilization, helping to delocalize the "extra" electron pair in the virtual orbitals. Based on the understanding gathered in this work, a set of organic molecules containing planar and neutral trivalent oxygen is theoretically proposed for the first time.

1. Introduction

Oxygen is one of the most abundant chemical elements on Earth and it is essential for life. It forms a rich variety of functional groups in organic compounds which are involved in many biochemical processes, such as the Krebs cycle and photosynthesis. As a general rule, oxygen behaves as a divalent atom; either forming one double bond as in the case of O_2 and carbonyls, or two single bonds as in H_2O, hydroxyls and ethers. Nonetheless, there are a number of remarkable exceptions to this rule: molecules containing oxonium ions, *i.e.*, positively charged trivalent oxygen. The best known and simplest case is the hydronium molecule (H_3O^+), where oxygen is coordinated to three hydrogen atoms. Oxonium ions are generally highly unstable and reactive, being relevant as reaction intermediates or synthetic reagents. Although these species can be isolated in

the form of oxonium salts (Meerwein salts) using non-nucleophilic counterions such as BF_4^- and PF_6^-, they still possess very high reactivity. However, Mascal *et al.* reported the synthesis and characterization of a new type of oxonium ion, *i.e.*, oxatriquinane and oxatriquinacene, which are surprisingly stable. In these molecules the O^+ ion is stabilized by fusing it inside a tricyclic condensed ring.[2–4] The lack of reactivity of these species against nucleophilic attack is associated with the ring strain, revealing the potential of embedding oxonium ions in ring frameworks for their stability. Subsequently, an oxatriquinane with a hydroxyl group in the α-position to oxygen was found to possess the longest C–O bond length reported to date (1.658 Å).[5] Steric repulsion and strong donation from oxygen non-bonding orbitals to adjacent σ*(C–O⁺) were argued to be the reasons for such C–O bond lengthening. These findings have encouraged the exploration of a plethora of new analogous oxonium ions.[6–13] However, it should be emphasized that, to the best of our knowledge, in all the molecules containing trivalent oxygen, O is positively charged and tetrahedral due to the sp³ hybridization. There are only three exceptions to this rule: Al_3O, Tl_3O and Ga_3O.[14–16] These three inorganic molecules were theoretically hypothesized to adopt a T-shape configuration with a planar tricoordinated oxygen (Al_3O can also adopt a Y-shape configuration).[14]

Oxygen functionalization in graphene has also been subject of numerous studies, due to the relevance for the processing of graphene oxide (GO) and its influence in the performance of supercapacitors, batteries, and electrocatalysts.[17–28] Functionalization of graphene with oxygen leads to an effective way of binding cations, which can either be part of the electrochemical

[a]Polimero eta Material Aurreratuak: Fisika, Kimika eta Teknologia Saila, Kimika Fakultatea, Euskal Herriko Unibertsitatea (UPV/EHU), M. de Lardizabal Pasealekua 3, Donostia, Euskadi, Spain. E-mail: elisa.jimenez@ehu.es

[b]Donostia International Physics Center (DIPC), Manuel de Lardizabal Pasealekua 3, Donostia, Euskadi, Spain. E-mail: wmbgalea@ehu.eus

[c]Department of General Chemistry (ALGC), Vrije Universiteit Brussel (VUB), Pleinlaan 2, 1050 Brussels, Belgium

[d]Institute of Advanced Synthesis, School of Chemistry and Molecular Engineering, Jiangsu National Synergetic Innovation Center for Advanced Materials, Nanjing Tech University, Nanjing 211816, China

[e]Fachbereich Chemie, Philipps-Universität Marburg, Hans-Meerwein-Strasse, D-35043 Marburg, Germany

[f]IKERBASQUE, Basque Foundation for Science, Euskadi, Bilbao, Spain

† Electronic supplementary information (ESI) available. See DOI: https://doi.org/10.1039/d4sc00142g

reactions or serve as anchors for metals.[29] Recently, Hofer *et al.* explored the possible binding configurations of oxygen in GO. Individual oxygen atoms were directly visualized using aberration-corrected scanning transmission electron microscopy (STEM) and single-atom electron energy loss spectroscopy (EELS).[1] In most cases oxygen was bound to two neighboring carbon atoms, as usual. Unexpectedly, however, in some cases oxygen was bonded to three carbons forming three equivalent bonds, a finding of great importance due to the rarity of this species. The electronic and transport properties of this system were later investigated. It was found that the tricoordinated oxygen acts as a n-type dopant, which is in contrast to the usual p-type oxygen bonded to the basal plane of graphene.[30]

However, it is unclear how oxygen binds to graphene in this configuration. Unlike molecular oxonium ions, the oxygen atom is not positively charged; it displays planar or quasi-planar coordination, and it is integrated into an extended system. These features make the chemical arrangement of oxygen unique. The present work aims at unveiling the chemical bonding of this atypical species. We believe such understanding will open the door to the development of new chemical species that can be integrated into different extended systems, to modulate at will their physico-chemical properties.

2. Methods

Periodic density functional theory (DFT) calculations were carried out with the PBE exchange–correlation functional[31,32] and projector augmented wave (PAW) pseudopotentials,[33] as implemented in the VASP code.[34–37] The planewave kinetic energy cutoff was set to 450 eV, and the convergence criteria for geometry (SCF) relaxation was set to 10^{-5} (10^{-6}) eV. The Brillouin zone was sampled with a $5 \times 5 \times 1$ Monkhorst–Pack k-grid. The DFT-D3 scheme was used to account for the dispersion interactions.[38] The system was modeled using a 6×6 oxygen monodoped graphene supercell of 72 atoms. In this cell, a single oxygen atom equates to a concentration of 1.4%. A vacuum separation of at least 15 Å was added in the z direction to avoid self-interaction with repeating images. To study the electronic structure in greater detail, projected crystal orbital Hamilton population (pCOHP) analysis was performed by means of the LOBSTER program.[39–42] The pCOHP is a very useful tool to discern the bonding/antibonding character of the interaction between specific pairs of atoms. For these calculations, the sigma value was reduced to 0.05 eV and a finer k-grid of $36 \times 36 \times 1$ was used.

Considered molecules were modeled with the Gaussian 16 package[43] using the CAM-B3LYP[44] functional. Geometry optimizations were carried out with the 6-31G[45] basis set whereas delocalization indices and Bader charges were computed using the 6-311G(d,p) basis set.[46] The bonding analysis was done with the Adaptive Natural Density Partitioning (AdNDP) method.[47] AdNDP partitions the electron density matrix into n centers and 2 electrons (nc–$2e$) bonds. Furthermore, AdNDP was shown to be nearly basis-set independent, and hence the CAM-B3LYP functional was used together with a smaller 6-31G basis set.

The calculation of the delocalization indices (DIs) employs the atomic partitions from the quantum theory of atoms in molecules (QTAIM),[48] as obatained with the AIMAll software.[49] The delocalization index (DI)[50–52] between two different atoms (A and B) is defined as:

$$\delta(A, B) = 2 \int_A \int_B d_1 d_2 \rho_{xc}(1, 2) = -2 \, \mathrm{cov}(N_A, N_B) \qquad (1)$$

where ρ_{xc} is the exchange–correlation density and N_A is the atomic population of atom A. The delocalization index is related to the covariance of these populations, and for this reason, the DI is a measure of the number of electrons fluctuating concurrently between these atoms.

NBO[53] and EDA-NOCV[54–56] calculations were carried out at the BP86-D3(BJ)/def2-TZP level of theory.[57,58] This method combines the energy decomposition analysis with the natural orbitals for chemical valence and decomposes the interaction energy (ΔE_{int}) between two fragments into four energy components, namely, the electrostatic interaction (ΔE_{elstat}), Pauli repulsion (ΔE_{Pauli}), attractive orbital interactions (ΔE_{orb}), and the dispersion interaction (ΔE_{disp}) :

$$\Delta E_{int} = \Delta E_{elstat} + \Delta E_{Pauli} + \Delta E_{orb} + \Delta E_{disp} \qquad (2)$$

3. Results

First, the tricoordinated oxygen embedded in graphene, the so-called graphitic oxygen, was characterized using a slab model and plane-waves DFT (PW-DFT). This configuration can be considered as a substitutional doping of oxygen in pristine graphene. As shown in Fig. 1, oxygen is located 0.20 Å above the plane, in agreement with the work by Hofer *et al.*[1] It forms three symmetrical bonds with the nearest carbon atoms, with bond lengths of 1.49 Å. These bond lengths are larger than the C–O bonds in ordinary ethers, ~1.43 Å, a feature found in molecules containing tricoordinated oxygen.[4] The lengthening of the bond
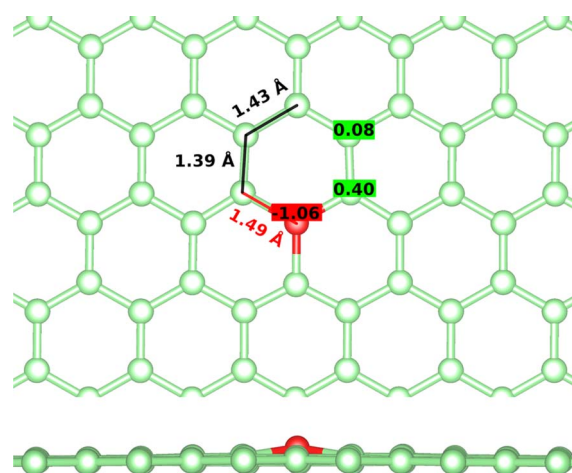

Fig. 1 Optimized structure of graphitic oxygen along with the bond lengths (in Å) and Bader charges. Top view of the structure on top, and side view on the bottom. Carbon and oxygen atoms are depicted in green and red, respectively.

has previously been ascribed to the filling of the σ^*(C–O) anti-bonding molecular orbital (MO).[4] In addition, the carbon atoms directly bonded to oxygen form a shrunken bond with their adjacent carbon atoms of *ca.* 1.39 Å, whereas the latter carbon atoms form slightly larger C–C bonds (1.43 Å *vs.* 1.42 Å in pristine graphene). The relaxed scan in Fig. S1† shows that the out-of-plane structure is a minimum in the potential energy surface of the system, whereas the completely planar structure is not. The computed Bader charges show that oxygen with-draws 1.06 $|e|$, mostly from the three closest carbon atoms. In this line, local charge depletion areas can also be observed between the C and O atoms and in the closest C atoms, as indicated by the charge density distribution (CDD) in Fig. S2.†

The electronic structure is then studied in detail. The calculations reveal a nonmagnetic structure for the ground state. In order to analyze the chemical bonding in the graphitic oxygen, first a pCOHP analysis was performed, which partitions the band-structure in terms of orbital-pair contributions, discerning between bonding/antibonding contributions. This analysis suggests that the oxygen–graphene bonding can be divided into three components. On the one hand, Fig. 2b shows a σ contribution to the pCOHP between O and one of the closest C arising from their s, p_x and p_y atomic orbitals (AOs). A bonding overlap (–pCOHP > 0) was observed throughout the –16 to –10 eV energy range, corresponding to this C–O σ bond. This interaction, together with the quasi-planar geometry of the system, pinpoints to a sp^2 hybridization on oxygen. Additionally, the COHP was projected into the p_z AOs to analyze the π interactions. In Fig. 2c) the π contribution to the C–O_1 inter-action is shown, along with the pCOHP between pairs of the C

atoms in the O-containing ring (see Fig. 2a)). Two localized peaks appear at around –8.9 and –0.02 eV, indicating the presence of O p_z and C p_z AOs hybridization. The peak at –8.9 eV corresponds to a π bonding state (–pCOHP > 0) with contribution from O–C_1, as well as C_1–C_2 and C_2–C_3 pairs. Contrary to the previous case, in the π state at –0.02 eV the O and C p_z AOs overlap in an antibonding manner (–pCOHP < 0). At the same energy, the pCOHP of C_1–C_2 is bonding while that of C_2–C_3 becomes antibonding again. It can be concluded that the latter state presents alternating nodal planes between O and C_1 and C_2 and C_3 perpendicular to the basal plane. This anti-bonding π state is filled leading to the n-type behavior of oxygen, which is in agreement with previous work carried out on the same system.[30]

In order to gain a deeper understanding of the chemical bonding of the graphitic oxygen, a fragmental approach was used, which has been successfully applied in previous studies on graphene and boron α-sheets.[59,60] In our approach we studied five molecules, with the tricoordinated oxygen located in the center, adding one coordination sphere from the smallest molecule containing O. The set of molecules studied were: $[OC_{12}H_9]^{7+}$, $[OC_{36}H_{15}]^{13+}$, $[OC_{72}H_{21}]^{19+}$, $[OC_{120}H_{27}]^{25+}$ and $[OC_{180}H_{33}]^{31+}$. These molecules were built starting from the optimized periodic graphitic oxygen and freezing their geom-etry. As mentioned above, oxygen is slightly out of plane in graphitic oxygen, and it remains in this position in the fragment molecules (although as we will show, it has no effect on the chemical bonding). Hydrogen atoms were added to saturate the σ bonds of the peripheral carbon atoms. In the infinite gra-phene lattice, each carbon atom shares its π electrons with
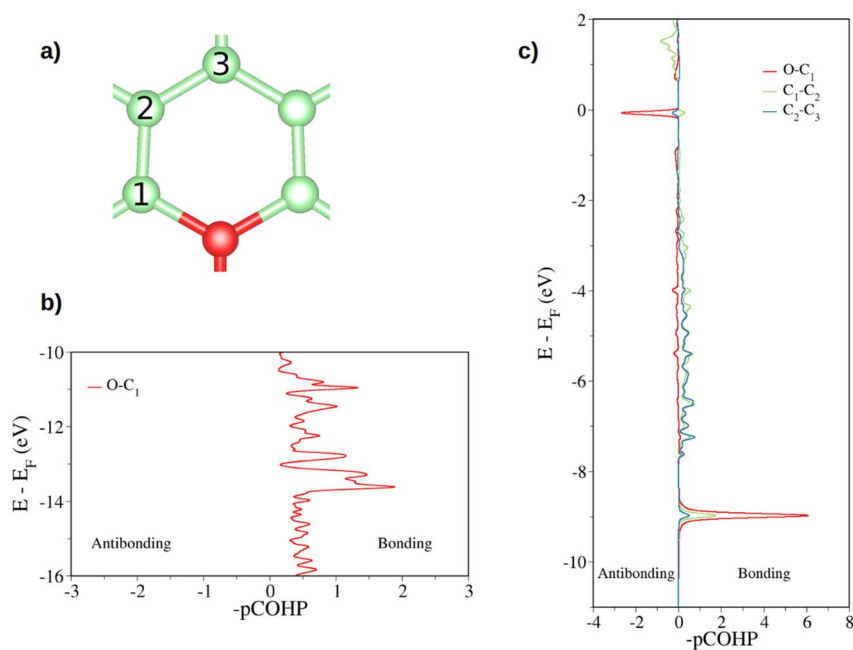

Fig. 2 Projected crystal orbital Hamilton population (pCOHP) plot between the different pairs of atoms is indicated (a). In (b) the COHP is projected onto the sum of s, p_x, p_y atomic orbitals of O and C while in (c) the total COHP is projected onto the atomic p_z orbitals (a pCOHP plot between C_1–C_2 p_z AOs can be seen in Fig. S3†). Positive –pCOHP values correspond to bonding interactions, while negative –pCOHP to antibonding interactions, respectively. The energy is given with respect to the Fermi energy (E_F).

three adjacent hexagons, contributing with only 1/3 of its π electrons to each hexagonal ring. Thus, in order to mimic the infinite graphene lattice, positive charges were added so that the number of π electrons in the periodic system were preserved.

First of all, Bader charges and delocalization indexes were computed in order to determine at which molecular size these electronic properties converge around oxygen. As shown in Fig. S4–S8,† the DIs of the atoms in the first coordination sphere converge at the intermediate $[OC_{72}H_{21}]^{19+}$ size. In this molecule the Bader charges also converged. Therefore, $[OC_{72}H_{21}]^{19+}$ was chosen as a model molecule to study how oxygen is bonded and stabilized in graphitic oxygen. It should be mentioned that the Electron Localization Function (ELF) was additionally plotted for both the extended surface and the $[OC_{72}H_{21}]^{19+}$ molecule and we concluded that this property is also converged at this molecular size. Further details can be found in the ESI (Section 5 and Fig. S9).†

The DI is a quantitative measure of the number of electron pairs that are delocalized or shared between two atoms. A value close to 1 is expected for an electron pair shared between two atoms, a 2-center 2-electron bond (2c–2e).[61] In benzene the DIs between pairs of C atoms is 1.40. In Fig. 3 the DIs of $[OC_{72}H_{21}]^{19+}$ are shown and compared with the analogous molecule made of all carbon atoms, $[C_{73}H_{21}]^{19+}$ (see Fig. S4–S8† for further details). The most significant difference between the two molecules was found at the DI between C–O vs. C–C (0.74 vs. 1.16). Such a low value in the C–O bond shows that the delocalization is lower in the hexagons containing oxygen. Moreover, a DI value smaller than 1.0 is indicative either of a strongly polarized bond or the population of antibonding orbitals.

The computed Bader charges on $[OC_{72}H_{21}]^{19+}$ are very similar to those obtained for the periodic system: $-0.93\ |e|$ on oxygen, $0.33\ |e|$ on the three closest carbon atoms, and $0.14\ |e|$ on the second nearest carbon atoms. We then performed a chemical bonding analysis on the $[OC_{72}H_{21}]^{19+}$ model fragment using the AdNDP tool,[47] which provides a description of localized and delocalized bonds by localizing the valence electrons in 1-center 2-electron bonds (1c–2e), 2-center 2-electron bonds (2c–2e), and n-center 2-electron bonds (nc–2e). As shown in Fig. 4, in our model molecule AdNDP localizes 96 2c–2e bonds between each adjacent C–C atoms (occupation numbers, ON = 1.99–1.97 $|e|$) and 21 2c–2e bonds between C and H atoms at the edges (ON = 1.98–1.97 $|e|$). In addition, oxygen forms three σ 2c–2e with the nearest carbon atoms (ON = 1.99 $|e|$). Due to the difference in electronegativity between carbon and oxygen (2.55 vs. 3.44), such C–O bonds will be polarized towards oxygen, explaining the negative charge on oxygen gained from these three closest carbon atoms.

Moreover, AdNDP shows that the additional two electrons contributed by oxygen are delocalized over a completely bonding 4c–2e bond, that involves the oxygen atom and the three nearest carbon atoms (ON = 1.99 $|e|$). With two delocalized electrons populating this bond, the system obeys the Hückel rule for aromaticity ($4n + 2$), with $n = 0$, making the system locally π aromatic. Aromaticity confers an enhanced stability on chemical systems and could explain, at least in part, the reason why, unlike other species in which oxygen is tricoordinated, in this case O has a sp^2 hybridization being almost planar. Indeed, this geometrical arrangement allows for the orbital overlap between oxygen and the three closest carbon atoms. We should highlight that the AdNDP analysis was also carried out on an analogous molecule, which is completely planar, and the results are identical.

The remaining electrons are delocalized over the hexagonal rings forming the π system. On the one hand, on each ring composed of only carbon atoms there is a 6c–2e bond (ON = 1.87–1.83 $|e|$), in agreement with previous works.[60] On the other hand, a 6c–2e bond is located (ON = 1.86 $|e|$) on each of the three hexagons containing oxygen. Note however, that unlike in the all-C rings where the bond is clearly fully bonding, in the O-containing rings the delocalized bond has an antibonding character, since oxygen is in antiphase with the rest of the electronic π cloud. This filling of the bonds with antibonding character is consistent with the fact that the DI value for the C–O bond is smaller than 1 as well as with the pCOHP analysis near the Fermi energy.
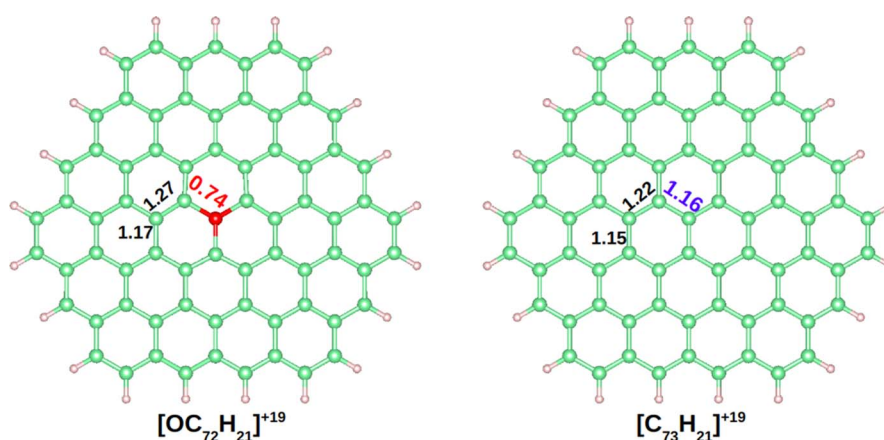

Fig. 3 Delocalization indexes on $[OC_{72}H_{21}]^{19+}$ and $[C_{73}H_{21}]^{19+}$. Carbon, hydrogen, and oxygen atoms are depicted in green, white and red, respectively.
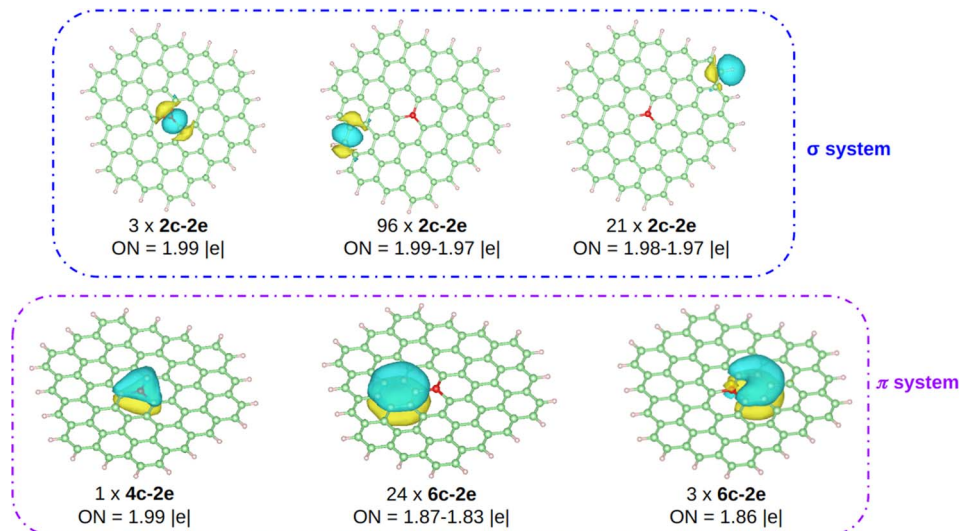
Fig. 4 AdNDP analysis on $[OC_{72}H_{21}]^{19+}$. Carbon, hydrogen, and oxygen atoms are depicted in green, white, and red, respectively.

Overall the bonding picture given by AdNDP on the fragment molecules can be easily reconciled with the pCOHP results obtained for the graphitic oxygen. According to both models, oxygen is bonded to the three nearest carbon atoms through C–O σ bonds, and π bonds with both bonding and antibonding character.

In order to tackle the influence of the π-conjugated system in the planarity of the trivalent oxygen, the previously built fragment molecules were relaxed at the CAM-B3LYP/6-31G level of theory, but in their neutral form (charge = 0). When they are neutral, these molecules have a doublet ground spin state. The smallest molecule, $OC_{12}H_9$, is unstable when it is planar and neutral. In other words, it is not a minimum on the potential energy surface. However, the remaining molecules, $OC_{36}H_{15}$, $OC_{72}H_{21}$, $OC_{120}H_{27}$, and $OC_{180}H_{33}$, are stable in the D_{3h} symmetry. The vibrational analysis confirmed that the resulting molecular geometries have no imaginary frequencies. The fact that trivalent oxygen cannot be stabilized in the planar and neutral form in $OC_{12}H_9$ suggests that a π-conjugated system is required to accept the "extra" electron pair brought by the O atom. According to our calculations $OC_{36}H_{15}$ is the smallest organic molecule, and the only molecule in which oxygen forms three equivalent bonds reported so far, that could accommodate a planar neutral trivalent oxygen.

Finally, the energy decomposition analysis with the combination of natural orbital for chemical valence (EDA-NOCV) calculations was carried out to complement the previous investigation. This method provides the most appropriate model to represent the bonding situation in the equilibrium geometry. The $[OC_{72}H_{21}]^{19+}$ cationic molecule was first optimized and it was found that the C_s and C_{3v} structures are nearly degenerate, while the D_{3h} form of the cation is 5.3 kcal mol^{-1} higher in energy. Nevertheless, as depicted in Tables S1 and S2† the EDA-NOCV calculations are nearly unchanged regardless of the symmetry of the molecule, as the bond lengths do not change and the core of the molecule remains planar.

EDA-NOCV results for the $[OC_{72}H_{21}]^{19+}$ molecule are shown in Table 1. The best bonding description emerges from the interaction between neutral O and the charged ligand, both in their triplet state. The energy decomposition analysis reveals that approximately 25% of the contribution to the total interaction energy comes from electrostatic forces and *ca.* 75% from the orbital interaction. Similarly, most of the orbital interaction is contributed by stabilizing σ interactions (ΔE_{orb1}, ΔE_{orb2} and ΔE_{orb3} in Table 1) between oxygen and the graphitic ligand. As shown in Fig. 5, S10 and S11,† the two nearly degenerate interactions, ΔE_{orb1} and ΔE_{orb2}, arise from the electron-sharing σ interaction of the singly occupied 2p AOs of O, while ΔE_{orb3} originates from a dative interaction of the doubly occupied 2s AO of O. Moreover, the deformation density suggests that the associated σ charge-donation mainly goes from the three directly bonded carbon atoms to the oxygen atom $[C_{72}H_{21}]^{+19} \rightarrow$ O, indicating that the highly charged ligand is a σ donor and the

Table 1 EDA-NOCV results of $[OC_{72}H_{21}]^{19+}$ (D_{3h}, S) at the BP86-D3(BJ)/def2-TZ2P level of theory. Fragments are given in singlet (S) or triplet (T) electronic states. Energy values are given in kcal mol^{-1}

Fragments	O(T) + $[C_{72}H_{21}]^{19+}$(T)	O(S) + $[C_{72}H_{21}]^{19+}$(S)
ΔE_{int}	−316.6	−954.5
ΔE_{Pauli}	475.0	286.5
ΔE_{elstat}[a]	−233.0 (29.4%)	−348.0 (28.0%)
ΔE_{disp}[a]	−2.8 (0.4%)	−2.8 (0.2%)
ΔE_{orb}[a]	−555.9 (70.2%)	−890.2 (71.7%)
ΔE_{orb1}[b]	−188.7 (33.9%)	
ΔE_{orb2}[b]	−188.3 (33.9%)	
ΔE_{orb3}[b]	−109.8 (19.8%)	
ΔE_{orb4}[b]	−27.2 (4.9%)	
$\Delta E_{orb(rest)}$[b]	−41.9 (7.5%)	

[a] The values in parentheses give the percentage contribution to the total attractive interactions $\Delta E_{elstat} + \Delta E_{orb} + \Delta E_{disp}$. [b] The values in parentheses give the percentage contribution to the total orbital interactions ΔE_{orb}.
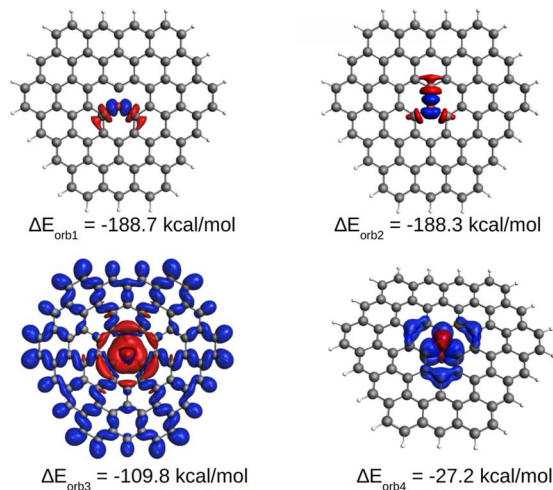
Fig. 5 Plot of deformation densities $\Delta\rho$ of the orbital interactions between the two fragments of O (T) and $[C_{72}H_{21}]^{19+}$(T) in $[OC_{72}H_{21}]^{19+}$ together with the associated interaction energies ΔE_{orb} (in kcal mol^{-1}). The direction of the charge flow is from red to blue.

$\Delta E_{orb1} = -188.7$ kcal/mol $\Delta E_{orb2} = -188.3$ kcal/mol
$\Delta E_{orb3} = -109.8$ kcal/mol $\Delta E_{orb4} = -27.2$ kcal/mol

neutral oxygen atom is a σ acceptor. This scenario correlates well with the previously proposed C–O σ bonds which are polarized, leading to a negative charge on O. This seemingly paradoxical charge migration becomes understandable when one realizes that the positive charge on the ligand is localized at the outermost atoms, revealing that the graphite ligand behaves like a Faraday cage. In addition to such a strong σ bonding associated with the ligand to oxygen donation, a comparatively weak π interaction is found in the opposite direction, *i.e.*, from oxygen to the ligand. ΔE_{orb4} comes from the π donation $[C_{72}H_{21}]^{19+} \leftarrow$ O. The shape of the deformation density indicates that the π donation from O to C essentially only affects the carbon atoms located in the three rings with a common oxygen atom in the center, as observed in the AdNDP analysis.

It is noteworthy that the $[OC_{36}H_{15}]^{+13}$ molecule was additionally tested in both the cationic and anionic forms. The EDA-NOCV results are shown in Fig. S12, S13, Tables S3 and S4.† The analysis reveals the same trends as in the larger molecule. Moreover, the bonding between oxygen and the graphitic ligand in the highly charged cation is very similar, in terms of total interaction as well as the type of interaction, to the neutral system. In fact, the interaction energies and the energy components are very similar. These results suggest that the effect of the charge is confined to the outer sphere, with a minor effect on the bonding in the center of the molecule, supporting the use of the fragmental approach to study the graphitic oxygen.

4. Conclusions

Oxygen is usually divalent, forming two chemical bonds, although there are a few exceptions to this rule among the known organic compounds: the hydronium molecule, H_3O^+, and oxonium salts. However, in the recent experimental finding by Hofer *et al.*[1] the tricoordinated oxygen embedded in

graphene is so striking because, unlike molecular oxonium ions, the oxygen atom is not positively charged, it displays planar or quasi-planar coordination and it is integrated into an extended system. These features make the chemical arrangement of oxygen unique. In this theoretical work, using a variety of state-of-the-art methods and combining periodic calculations with a fragmental approach we tried to unravel the factors influencing the stability of this exotic species. A σ-donation from the graphitic ligand to oxygen and a π-backdonation in the opposite direction are identified. Importantly, the electronic structure indicates aromatic stabilization for at least part of the regions of delocalized bonding. In fact, the system is found to have local π aromaticity, with a delocalized 4c–2e bond that involves the oxygen atom and the three nearest carbon atoms. Finally, the framework in which oxygen is embedded plays a pivotal role on the stabilization. In fact, the π-conjugated system helps to delocalize the "extra" electron pair in the virtual orbitals. In this way, a set of organic molecules containing planar and neutral trivalent oxygen is theoretically proposed for the first time.

Data availability

The data that support the findings of this study are available from the corresponding author upon reasonable request. The corresponding author, on behalf of all authors of the paper, is responsible for submitting a competing interests statement.

Author contributions

A. U. performed the calculations in the extended system and analyzed the results. I. C.-R. performed and analyzed the Bader charges and performed DI calculations, L. Z. and Z. Z. performed the EDA-NOCV calculations and analyzed the results, G. F. analyzed the EDA-NOCV results, J. M. U. supervised the work, A. G.-L. brought the inspiration and supervised the work, E. J.-I. performed and analyzed the AdNDP calculations and supervised the work. All the authors contributed to the writing of the work. All authors reviewed the manuscript.

Conflicts of interest

The authors declare no conflict of interest.

Acknowledgements

References

1 C. Hofer, V. Skákalová, T. Görlich, M. Tripathi, A. Mittelberger, C. Mangler, M. R. A. Monazam, T. Susi, J. Kotakosk and J. C. Meyer, Direct imaging of light-element impurities in graphene reveals triple-coordinated oxygen, *Nat. Commun.*, 2019, **10**, 4570–4577.

2 M. Mascal, N. Hafezi, N. K. Meher and J. C. Fettinger, Oxatriquinane and Oxatriquinacene: Extraordinary Oxonium Ions, *J. Am. Chem. Soc.*, 2008, **130**, 13532–13533.

3 M. Haley, Taming the Highly Reactive Oxonium Ion, *Angew. Chem., Int. Ed.*, 2009, **48**, 1544–1545.

4 G. Gunbas, N. Hafezi, W. L. Sheppard, M. M. Olmstead, I. V. Stoyanova, F. S. Tham, M. P. Meyer and M. Mascal, Extreme oxatriquinanes and a record C-O bond length, *Nat. Chem.*, 2012, **4**, 1018–1023.

5 G. Gunbas, W. L. Sheppard, J. C. Fettinger, M. M. Olmstead and M. Mascal, Extreme Oxatriquinanes: Structural Characterization of α-Oxyoxonium Species with Extraordinarily Long Carbon–Oxygen Bonds, *J. Am. Chem. Soc.*, 2013, **135**, 8173–8176.

6 H. Suzuki and H. Muratake, Functionalized oxatriquinanes and their structural equilibrium in protic solvent, *Chem. Pharm. Bull.*, 2014, **62**(9), 921–926.

7 E. S. Stoyanov, G. Gunbas, N. Hafezi, M. Mascal, I. V. Stoyanova, F. S. Tham and C. A. Reed, The $R_3O^+\cdots H^+$ Hydrogen Bond: Toward a Tetracoordinate Oxadionium(2+) Ion, *J. Am. Chem. Soc.*, 2012, **134**, 707–714.

8 H. Suzuki and H. Muratake, Functionalized oxatriquinanes and their structural equilibrium in protic solvent, *Chem. Pharm. Bull.*, 2014, **62**, 921–926.

9 H. S. S. Chan, Q. N. N. Nguyen, R. S. Paton and J. W. Burton, Synthesis, characterization and reactivity of complex tricyclic oxonium ions, proposed intermediates in natural product biosynthesis, *J. Am. Chem. Soc.*, 2019, **141**(40), 15951–15962.

10 I. Novak, Computational thermochemistry of oxatriquinane and its analogues, *Comput. Theor. Chem.*, 2019, **1147**, 35–39.

11 O. Smith, M. V. Popescu, M. J. Hindson, R. Paton, J. W. Burton and M. D. Smith, Control of stereogenic oxygen in a helically chiral oxonium ion, *Nature*, 2023, **615**, 430–435.

12 N. Hafezi and M. Mascal, Chemistry of the Heterotriquinanes and Heterotriquinacenes, *Synlett*, 2022, **33**, 231–246.

13 S. J. Grabowski, E. Formoso, D. Casanova and J. M. Ugalde, Tetravalent Oxygen and Sulphur Centres Mediated by Carborane Superacid: Theoretical Analysis, *ChemPhysChem*, 2019, **20**, 2443–2450.

14 A. I. Boldyrev and P. v. R. Schleyer, Ab Initio Prediction of the Structures and Stabilities of the Hyperaluminum Molecules: Al_3O and Square-Planar Al_4O, *J. Am. Chem.*, 1991, **113**, 9045–90544.

15 K. Zhou, S. K. Roy and C. B. Zhao, Ga_xO (x = 2–4) Contain Novel Linear Dicoordinate, T-shape Tricoordinate and Planar Tetracoordinate Oxygen, *Russ. J. Inorg. Chem.*, 2019, **64**, 303–307.

16 K. Zhou, S. Roy and C.-B. Zhao, Tl_xO (x = 2–4) contain novel linear di-coordinated, T-shaped tri-coordinated and square-planar tetra-coordinated oxygen, *Comput. Theor. Chem.*, 2017, **1110**, 35–39.

17 X. Lu, W.-L. Yim, B. H. R. Suryanto and C. Zhao, Electrocatalytic Oxygen Evolution at Surface-Oxidized Multiwall Carbon Nanotubes, *J. Am. Chem. Soc.*, 2015, **137**(8), 2901–2907.

18 Z. Lu, G. Chen, S. Siahrostami, Z. Chen, K. Liu, J. Xie, L. Liao, T. Wu, D. Lin, Y. Liu, T. F. Jaramillo, J. K. Nørskov and Y. Cui, High-efficiency oxygen reduction to hydrogen peroxide catalysed by oxidized carbon materials, *Nat. Catal.*, 2018, **1**(2), 156–162.

19 F. Yang, X. Ma, W.-B. Cai, P. Song and W. Xu, Nature of Oxygen-Containing Groups on Carbon for High-Efficiency Electrocatalytic CO2 Reduction Reaction, *J. Am. Chem. Soc.*, 2019, **141**(51), 20451–20459.

20 Z. Liu, Z. Zhao, Y. Wang, S. Dou, D. Yan, D. Liu, Z. Xia and S. Wang, In Situ Exfoliated, Edge-Rich, Oxygen-Functionalized Graphene from Carbon Fibers for Oxygen Electrocatalysis, *Adv. Mater.*, 2017, **29**(18), 1606207.

21 J. Yan, Q. Wang, T. Wei, L. Jiang, M. Zhang, X. Jing and Z. Fan, Template-Assisted Low Temperature Synthesis of Functionalized Graphene for Ultrahigh Volumetric Performance Supercapacitors, *ACS Nano*, 2014, **8**(5), 4720–4729.

22 B. Liu, B. Y. Liu, H. Chen, M. Yang and H. Li, Oxygen and nitrogen co-doped porous carbon nanosheets derived from Perilla frutescens for high volumetric performance supercapacitors, *J. Power Sources*, 2017, **341**, 309–317.

23 P. Cai, K. Zou, G. Zou, H. Hou and X. Ji, Quinone/ester-based oxygen functional group-incorporated full carbon Li-ion capacitor for enhanced performance, *Nanoscale*, 2020, **12**(6), 3677–3685.

24 I. K. Ilic, K. Leus, J. Schmidt, J. Hwang, M. Maranska, S. Eigler and C. Liedel, Polymerization in Carbone: A Novel Method for the Synthesis of More Sustainable Electrodes and Their Application as Cathodes for Lithium–Organic Energy Storage Materials Based On Vanillin, *ACS Sustainable Chem. Eng.*, 2020, **8**(8), 3055–3064.

25 C. Matei Ghimbeu, J. Górka, V. Simone, L. Simonin, S. Martinet and C. Vix-Guterl, Insights on the Na+ ion storage mechanism in hard carbon: Discrimination between the porosity, surface functional groups and defects, *Nano Energy*, 2018, **44**, 327–335.

26 X. Chen, X.-R. Chen, T.-Z. Hou, B.-Q. Li, X.-B. Cheng, R. Zhang and Q. Zhang, Lithiophilicity chemistry of heteroatom-doped carbon to guide uniform lithium nucleation in lithium metal anodes, *Sci. Adv.*, 2019, **5**(2), eaau7728.

27 X. Zhu, K. Liu, Z. Lu, Y. Xu, S. Qi and G. Zhang, Effect of oxygen atoms on graphene: Adsorption and doping, *Phys. E*, 2020, **117**, 113827.

28 A. F. Jiménez-González, J. M. Ramírez-de-Arellano and L. F. Magaña, Substantial Variations in the Optical Absorption and Reflectivity of Graphene When the Concentrations of Vacancies and Doping with Fluorine, Nitrogen, and Oxygen Change, *Int. J. Mol. Sci.*, 2021, **22**, 6832–6848.

29 M. Jerigová, M. Odziomek and N. López-Salas, "We Are Here!" Oxygen Functional Groups in Carbons for Electrochemical Applications, *ACS Omega*, 2022, **7**, 11544–11554.

30 D. M. A. Mackenzie, M. Galbiati, X. D. de Cerio, I. Y. Sahalianov, T. M. Radchenko, J. Sun, D. Peña, L. Gammelgaard, B. S. Jessen, J. D. Thomsen, P. Bøggild, A. Garcia-Lekue, L. Camilli and J. M. Caridad, Unraveling the electronic properties of graphene with substitutional oxygen, *2D Mater.*, 2021, **8**, 045035–045043.

31 J. P. Perdew, K. Burke and M. Ernzerhof, Generalized gradient approximation made simple, *Phys. Rev. Lett.*, 1996, **77**, 3865–3868.

32 J. P. Perdew, K. Burke and M. Ernzerhof, Perdew, Burke, and Ernzerhof reply, *Phys. Rev. Lett.*, 1997, **78**, 1396.

33 G. Kresse and D. Joubert, From ultrasoft pseudopotentials to the projector augmented-wave method, *Phys. Rev. B: Condens. Matter Mater. Phys.*, 1999, **59**, 1758–1775.

34 G. Kresse and J. Hafner, Ab initio molecular dynamics for liquid metals, *Phys. Rev. B: Condens. Matter Mater. Phys.*, 1993, **47**, 558–561.

35 G. Kresse and J. Hafner, Ab initio molecular-dynamics simulation of the liquid-metal–amorphous-semiconductor transition in germanium, *Phys. Rev. B: Condens. Matter Mater. Phys.*, 1994, **49**, 14251–14269.

36 G. Kresse and J. Furthmüller, Efficiency of ab-initio total energy calculations for metals and semiconductors using a plane-wave basis set, *Comput. Mater. Sci.*, 1996, **6**, 15–50.

37 G. Kresse and J. Furthmüller, Efficient iterative schemes for *ab initio* total-energy calculations using a plane-wave basis set, *Phys. Rev. B: Condens. Matter Mater. Phys.*, 1996, **54**, 11169–11186.

38 S. Grimme, J. Antony, S. Ehrlich and H. Krieg, A consistent and accurate ab initio parametrization of density functional dispersion correction (DFT-D) for the 94 elements H-Pu, *J. Chem. Phys.*, 2010, **132**, 154104–154122.

39 R. Dronskowski and P. E. Blöchl, Crystal orbital Hamilton populations (COHP): energy-resolved visualization of chemical bonding in solids based on density-functional calculations, *J. Phys. Chem.*, 1993, **97**, 8617–8624.

40 S. Maintz, V. L. Deringer, A. L. Tchougréeff and R. Dronskowski, LOBSTER: A tool to extract chemical bonding from plane-wave based DFT, *J. Comput. Chem.*, 2016, **37**, 1030–1035.

41 S. Maintz, V. L. Deringer, A. L. Tchougréeff and R. Dronskowski, Analytic projection from plane-wave and PAW wavefunctions and application to chemical-bonding analysis in solids, *J. Comput. Chem.*, 2013, **34**, 2557–2567.

42 V. L. Deringer, A. L. Tchougreeff and R. Dronskowski, Crystal Orbital Hamilton Population (COHP) Analysis As Projected from Plane-Wave Basis Sets, *J. Phys. Chem. A*, 2011, **115**, 5461–5466.

43 M. J. Frisch, G. W. Trucks, H. B. Schlegel, G. E. Scuseria, M. A. Robb, J. R. Cheeseman, G. Scalmani, V. Barone, G. A. Petersson, H. Nakatsuji *et al.*, *Gaussian 16 Revision C.01*, Gaussian Inc., Wallingford, CT, USA, 2016.

44 T. Yanai, D. P. Tew and N. C. Handy, A new hybrid exchange–correlation functional using the Coulomb-attenuating method (CAM-B3LYP), *Chem. Phys. Lett.*, 2004, **393**, 51–57.

45 R. Ditchfield, W. J. Hehre and J. A. Pople, Self-Consistent Molecular Orbital Methods. 9. Extended Gaussian-type basis for molecular-orbital studies of organic molecules, *J. Chem. Phys.*, 1971, **54**, 724.

46 W. J. Hehre, R. Ditchfield and J. A. Pople, *J. Chem. Phys.*, 1972, **56**, 2257–2261; W. J. Hehre, L. Radom, P. V. R. Schleyer and J. A. Pople, *Ab Initio Molecular Orbital Theory*, Wiley, New York, 1986.

47 D. Y. Zubarev and A. I. Boldyrev, Developing paradigms of chemical bonding: Adaptive natural density partitioning, *Phys. Chem. Chem. Phys.*, 2008, **10**, 5207–5217.

48 R. F. W. Bader, *Atoms in Molecules: A Quantum Theory*, Oxford University Press, Oxford, 1990.

49 T. A. Keith, *AIMAll (Version 14.11.23), 2014, tK Gristmill Software*, Overland Park KS, USA, https://aim.tkgristmill.com/.

50 X. Fradera, M. A. Austen and R. F. W. Bader, The Lewis model and beyond, *J. Phys. Chem. A*, 1999, **103**, 304–314.

51 X. Fradera, J. Poater, S. Simon, M. Duran and M. Solà, Electron-pairing analysis from localization and delocalization indices in the framework of the atoms-in-molecules theory, *Theor. Chem. Acc.*, 2002, **108**, 214–224.

52 J. Poater, X. Fradera, M. Solà, M. Duran and S. Simon, On the electron-pair nature of the hydrogen bond in the framework of the atoms in molecules theory, *Chem. Phys. Lett.*, 2003, **369**, 248–255.

53 (*a*) C. R. Landis and F. Weinhold, The NBO View of Chemical Bonding, in *The Chemical Bond: Fundamental Aspects of Chemical Bonding*, ed. G. Frenking and S. Shaik, Wiley-VCH, Weinheim, 2014, pp. 91–120; (*b*) F. Weinhold and C. R. Landis, *Discovering Chemistry With Natural Bond Orbitals*. Wiley, New Jersey, 2012; (*c*) C. R. Landis and F. Weinhold, *Valency and Bonding: A Natural Bond Orbital Donor-Acceptor Perspective*, Cambridge University Press, Cambridge, 2005.

54 F. M. Bickelhaupt and E. J. Baerends, Kohn-Sham Density Functional Theory: Predicting and Understanding Chemistry, *Rev. Comput. Chem.*, 2000, **15**, 1.

55 M. Mitoraj and A. Michalak, Donor–Acceptor Properties of Ligands from the Natural Orbitals for Chemical Valence, *Organometallics*, 2007, **26**, 6576.

56 P. Jerabek, P. Schwerdtfeger and G. Frenking, Dative and Electron-Sharing Bonding in Transition Metal Compounds, *J. Comput. Chem.*, 2019, **40**, 247.

57 A. D. Becke, Density-functional exchange-energy approximation with correct asymptotic behavior, *Phys. Rev. A*, 1988, **38**, 3098–3100.

58 F. Weigend and R. Ahlrichs, Energy-adjusted ab initio pseudopotentials for the second and third row transition elements, *Phys. Chem. Chem. Phys.*, 2005, **7**, 3297–3305.

59 I. A. Popov, T. R. Galeev, Q. Chen, J. C. Guo, H. Bai, C. Q. Miao, H. G. Lu, A. P. Sergeeva, S. D. Li and A. I. Boldyrev, Deciphering the mystery of hexagon holes in an all-boron graphene α-sheet, *Phys. Chem. Chem. Phys.*, 2011, **13**, 11575–11578.

60 I. A. Popov and K. V. Bozhenko, A. I. BoldyrevIs Graphene Aromatic?, *Nano Res.*, 2012, **5**(2), 117–123.

61 E. Matito and M. Sol, The role of electronic delocalization in transition metal complexes from the electron localization function and the quantum theory of atoms in molecules viewpoints, *Coord. Chem. Rev.*, 2009, **253**, 647–665.